Magnetic Characteristics of High-power-density In-wheel Motor using Halbach Magnet Array

Makoto Ito [1)] Tetsuya Suto [1)] Akeshi Takahashi [1)] Takafumi Hara [2)] Ryuichiro Iwano [1)]

1) Hitachi, Ltd., Research and Development Group, Hitachi, Ibaraki, Japan

E-mail: makoto.ito.wg@hitachi.com

2) Hitachi Astemo, Ltd., Hitachinaka, Ibaraki, Japan

ABSTRACT: We are developing compact and lightweight in-wheel motors that can increase the cruising range for electric vehicles which are becoming more prevalent in the decarbonized society. This paper proposes a Halbach magnet array to achieve a world-class motor power density of 2.5 kW/kg. Finite element method analysis shows that our Halbach magnet array can obtain a large gap magnetic flux density with a small amount of magnets compared with the conventional Halbach rotor with a surface-permanent-magnet layout.

KEY WORDS: electric vehicle, in-wheel motor, Halbach magnet arrays

1. INTRODUCTION

Much money and effort have been invested into developing technology for a decarbonized society. In the automotive industry, laws and regulations to move from gasoline-powered vehicles to electric vehicles (EVs) are being enacted in many countries. Conventional EVs, however, have a drive system on the chassis, which limits the vehicle space including the battery-installation space. Therefore, not enough batteries can be installed to make EVs suitable for long-distance running. This short cruising distance inhibits their wider adoption. In-wheel motors are attracting attention because they can expand the vehicle space by mouting the motor in the wheel[(1)]. However, in the conventional in-wheel motor, the large motor volume in the wheel (that is, the small output density) increases the weight under the spring. Solving this requires completely changing the suspension[(2)].

To solve this problem, various high-output technologies have been proposed, for example, interior permanent magnet synchronous motors[(3)-(9)], spoke motors[(10),(11)], and Halbach magnetized and Halbach array field motors[(12)-(15)]. However, previous studies have not taken a broad approach to motor design suitable for in-wheel motors.

On the basis of the above background, we clarified a strategy to increase the output density of in-wheel motors and investigated Halbach magnet arrays that can produce high power density of in-wheel motors. We first propose a Halbach magnet array to increase the motor torque by multi-polarization and increase tha gap magnetic flux density. Our Halbach magnet array rotor is characterized by having cores at the center of the pole, unlike a conventional Halbach rotor with a surface permanent magnet (SPM) layout. We then developed a rotor that includes our Halbach magnet array and determined its superiority by comparing it with a Halbach-array rotor with an SPM layout used for common multi-polar motors through finite element method (FEM) analysis and a simplified magnetic circuit model. Finally, we present the results of evaluating a prototype in-wheel motor that includes the developed rotor with our Halbach magnet array.

2. STRATEGY FOR HIGH POWER DENSITY

The magnitude of a motor's torque T is typically proportional to the product of the motor size, specific electrical load A_1, and specific magnetic load B_{av}. Using the following torque equation, the relationship between torque density and pole pair p can be investigated.

$$T \propto D_\delta^2 L A_1 B_{av} \tag{1}$$

Here, D_δ is the gap diameter, and L is the core thickness. The A_1 and B_{av} can be expressed as

$$A_1 = \frac{6N_{ph}I_{1n}}{\pi D_\delta}, \quad B_{av} = \frac{\phi_\delta}{\tau_p L} \tag{2}$$

where, N_{ph} is the number of turns in a phase, I_{1n} is the fundamental wave component of the rated current, ϕ_δ is the gap magneitc flux per pole, and τ_p is the polar pitch.

On the bases of Eqs. (1)–(3), we investigated the relationship between torque density and p. Assuming an in-wheel motor for EVs, D_δ was set to 300 mm, and L was set to 50 mm. As the restrict conditions, the magnetic flux density in the stator back

yoke was set to 1.2 T, and the current density of the winding was set to 20 A/mm^2. The A_1 was 1.0×10^5 A/m assuming large torque, and two gap magnetic flux densities of 0.8 T and 1.2 T were compared. The torque density and stator back yoke width were both 1.0 pu for $p = 1$ with the gap magnetic flux density of 0.8 T.

The relationship between the stator back yoke width and torque density with respect to p is shown in Fig. 1. When p is small, the amount of magnetic flux across the adjacent poles becomes large, which widens the stator back yoke. The back yoke can be narrowed when p is large. Therefore, by increasing p, the size and weight of the motor can be reduced, increasing the torque density. When the gap magnetic flux density is larger, the back yoke is wider, but the torque per unit core thickness is increased, so the torque density can be increased.

The sensitivity of torque density to gap magnetic flux density is more pronounced in multi-polarization. The above factors indicate that it is effective to make a motor multi-polar; thus, high torque density can be obtained by the synergistic effect of the multi-polarization of the motor and increase in the gap magnetic flux density. In the next chapter, we introduce our Halbach magnet array to effectively increase the gap magnetic flux density.

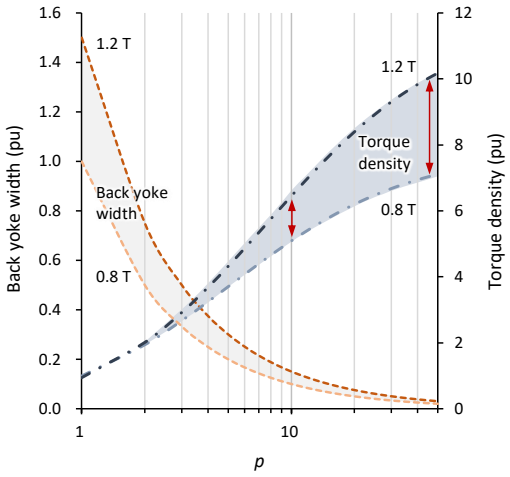

Fig. 1 Back yoke width and torque density with respect to number of p.

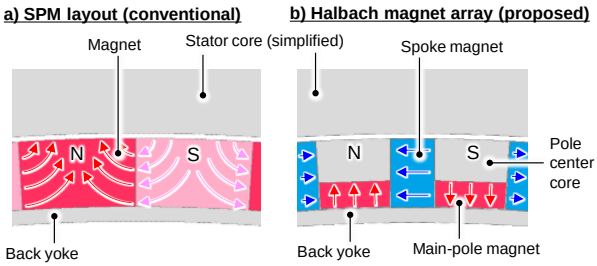

Fig. 2 Rotor models (left: SPM, right: Halbach array).

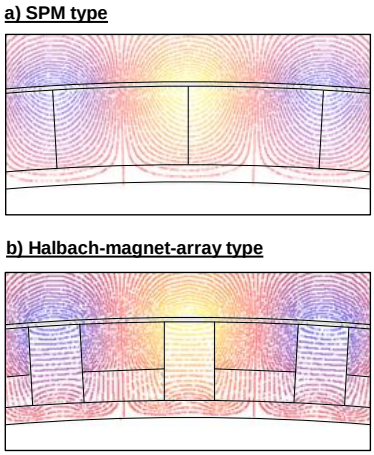

Fig. 3 Flux distribution (upper: SPM rotor, lower: Halbach magnet array rotor).

3. HALBACH ARRAYS

3.1. Finite-element-method analysis

Conventionally, a Halbach array is capable of inreasing the gap magnetic flux density. This is possible by providing a magnetization distribution such that the magnetic flux is concentrated in the gap in the SPM layout. However, since the magnetic path inside the magnet becomes longer in such a layout, the magnetic resistance inside the magnet is large compared with the magnetic resistance of the gap. As a result, the permeance coefficient is lowered, and the magnet operating magnetic flux density at each part is lowered, so there is a concern that the gap magnetic flux density cannot be increased sufficiently.

Therefore, we developed a rotor with our Halbach magnet array consisting of flat plate-shaped main pole magnets, spoke magnets, and pole center cores placed in the center of the poles, as shown in Fig. 2.

Figure 3 shows the FEM analysis results of the gap magnetic flux density by the permanent magnets in the SPM-type and Halbach-magnet-array-type rotor models. When the spatial-distribution fundamental-wave effective value of the gap magnetic flux density of the SPM rotor was 1.00 pu, it was 1.06 pu in our Halbach-magnet-array rotor. The amount of magnets was 0.61 pu for our Halbach-magnet-array rotor and 1.00 pu for the SPM rotor. Therefore, our Halbach-magnet-array-type rotor can achieve a large gap magnetic flux density with a small amount of magnets compared with the conventional SPM-type rotor.

3.2. Analysis using magnetic circuit model

For a more comprehensive analysis, a magnetic circuit model was used to demonstrate the superiority of the proposed Halbach

magnet array. In this magnetic circuit design, the following assumptions were made to simplify the calculations.

A) The permeability of the core is infinite.
B) The rotor shape for one pole is approximated by a rectangle.
C) The shape of the stator is irrelevant.
D) Since the back yoke width of the rotor is also related to design items such as the connection with the housing, the rotor back yoke shape is not considered.

Figure 4 shows the magnetic circuit model for one pole, where d is the radial width of the rotor excluding the back yoke width, x is the magnetization direction width of the main pole magnet, and y is the magnetization direction width of the spoke magnets. Using rotor outer diameter D_{ro} and rotor inner diameter D_{ri}, the τ_p and d of the rotor excluding the back yoke are expressed as

$$\tau_p = \frac{\pi(D_{ro} + D_{ri})}{4p} \sim \frac{\pi D_{ro}}{2p}, \quad d = \frac{D_{ro} - D_{ri}}{2} - e \qquad (3)$$

where, e is the radial width of the rotor back yoke.

Applying Ampere's law to each magnetic flux loop shown in Fig. 4, the following equations are obtained.

Loop 1:

$$\left(\frac{B_r}{\mu_r} y - \phi_{y1} R_{y1}\right) = 2\phi_\delta R_\delta \qquad (4)$$

Loop 2:

$$2\left(\frac{B_r}{\mu_r}\frac{x}{2} - \phi_{x1} R_{x1}\right) = \phi_{y2}(2R_{x3} + R_{y2}) - \phi_{y1} R_{y1} \qquad (5)$$

Loop 3:

$$2\left(\frac{B_r}{\mu_r}\frac{x}{2} - \phi_{x2} R_{x2}\right) - \left(\frac{B_r}{\mu_r} y - \phi_{y2} R_{y2}\right) = -2\phi_{y2} R_{x3} \qquad (6)$$

where, B_r is the residual magnetic flux density of the permanent magnet, μ_r is the recoil permeability, ϕ_{x1} and ϕ_{x2} are the magnetic fluxes passing through the main pole magnet, ϕ_{y1} and ϕ_{y2} are the magnetic fluxes passing through the spoke magnet, ϕ_δ is the magnetic flux through the gap. From the magnetic circuit diagram, the gap magnetic flux per pole is represented as $2\phi_\delta$. The notations R_{x1}, R_{x2} and R_{x3} are the magnetic resistances of the main pole magnets, R_{y1} and R_{y2} are those of the spoke magnets, and R_δ is that of the gap.

$$R_{x1} = R_{x2} = R_x = \frac{x}{\mu_r(\tau_p - y)L}, \quad R_{x3} = \frac{\tau_p - y}{4\mu_r x L} \qquad (7)$$

$$R_{y1} = \frac{y}{\mu_r(d - x)L}, \quad R_{y2} = \frac{y}{\mu_r x L} \qquad (8)$$

$$R_\delta = \frac{2\delta}{\mu_0(\tau_p - y)L} \qquad (9)$$

where L is the stack thickness, δ is the gap length, and μ_0 is the vacuum permeability. There is the following relationship between

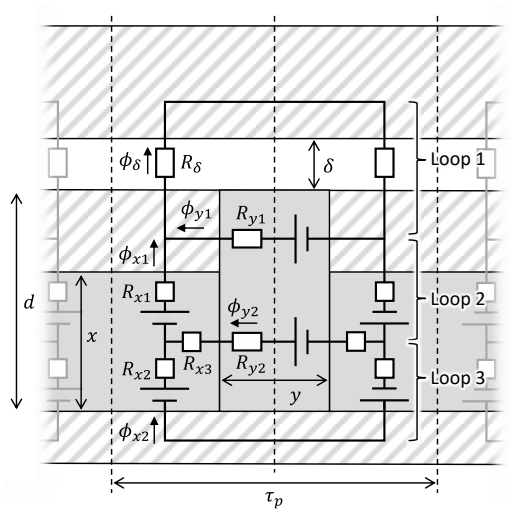

Fig. 4 Magnetic circuit model.

the magnetic flux passing through the gap and that passing through each magnet.

$$\phi_\delta = \phi_{x1} + \phi_{y1} \qquad (10)$$

$$\phi_{x1} = \phi_{x2} + \phi_{y2} \qquad (11)$$

From Eqs. (4)–(11), ϕ_δ can be obtained as a function of magnetic resistance and magnet width.

$$\phi_\delta = \frac{1}{\mathcal{R}}\frac{1}{R_x}\frac{B_r}{\mu_r} x + \frac{1}{\mathcal{R}}\left(\frac{1}{R'_{xy} + R_{xy}} + \frac{1}{R_{y1}}\right)\frac{B_r}{\mu_r} y \qquad (12)$$

where,

$$\mathcal{R} = 1 + \frac{R'_{xy} R_\delta}{R_{x1} R'_{xy} + R_{x2} R_{xy}} + \frac{2R_\delta}{R_{y1}} \qquad (13)$$

$$R_{xy} = 2R_{x3} + R_{y2}, \quad R'_{xy} = 2(R_{x2} + R_{x3}) + R_{y2} \qquad (14)$$

On the basis of the above, the total magnetic flux Φ_δ in the gap and gap magnetic flux density B_δ are expressed as follows.

$$\Phi_\delta = 2p \times 2\phi_\delta, \quad B_\delta = \frac{\Phi_\delta}{2p\tau_p L} \qquad (15)$$

Since B_δ in Eq. (15) is a function of the dimensional parameters of the magnet and core, the range of geometry parameters for maximizing the gap flux density can be determined.

Figure 5 shows the gap magnetic flux density map for the thickness of the main pole magnet and spoke magnets. The thickness of the magnets in the graph is standardized, and that of the main pole magnet x is 1 pu when it is equal to the radial thickness of the rotor, and the thickness of the spoke magnet y is 1 pu when it is equal to the pole pitch. That is, when x is 1 pu, the core at the pole center disappears and the magnet arrangement becomes similar to an SPM layout. This confirms that there is a set of magnet dimensions that maximizes the gap magnetic flux density in the range of $x < 1$ pu and $y < 1$ pu.

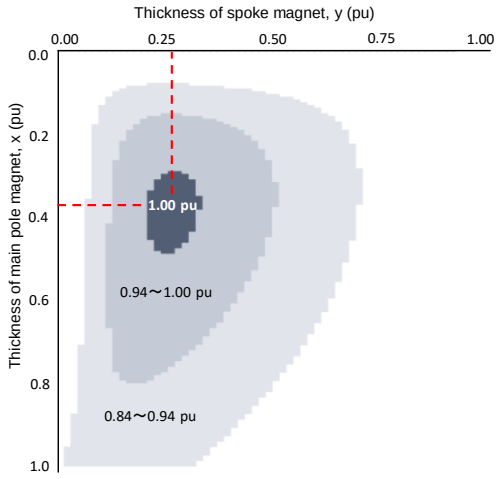

Fig. 5 Gap magnetic flux density map.

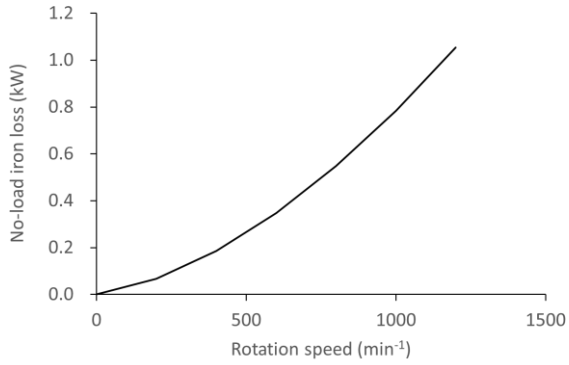

Fig. 6 Calculated no-load iron loss.

3.3. No-load iron loss

As the gap magnetic flux density increases, the no-load iron loss also increases. To quantify whether the no-load iron loss is acceptable, it was calculated using FEM analysis. Figure 6 shows the no-load iron loss versus rotation speed. The no-load iron loss at the rated speed of 600 min^{-1} was 347 W. Since the designed peak output is 60 kW, it can be said that the no-load iron loss is sufficiently small.

4. PROTOTYPE AND MEASUREMENT

4.1. Prototype in-wheel motor

We fabricated a prototype in-wheel motor using our Halbach-magnet-array rotor. Figure 7 shows the appearance of the motor including the inverter and developed rotor. The rotor is fixed to the shaft via a housing located on the inner circumference side, and power is transmitted to the wheel.

4.2. Measurement of no-load induced back electromotive force

The prototype was built into the test bench and the no-load loss and induced back electromotive force (EMF) was measured.

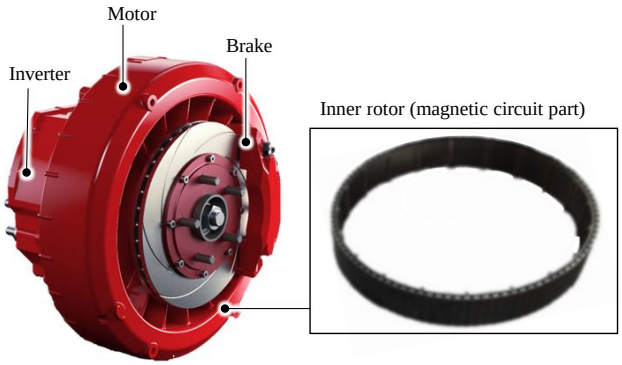

Fig. 7 Prototype in-wheel motor (left: external appearance, right: developed rotor).

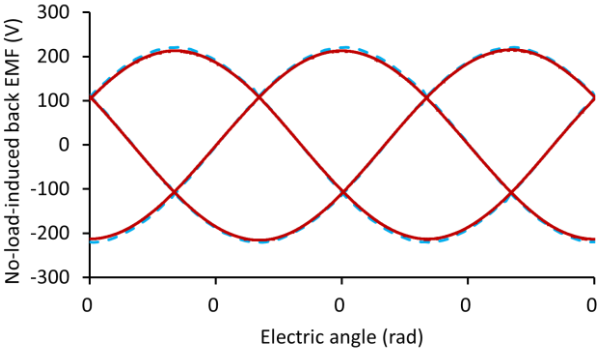

Fig. 8 Comparison of measured and calculated no-load-induced back EMF at 600 min^{-1}.

Figure 8 compares the measured waveform (solid line) and calculated waveform (dashed line) of the no-load-induced back EMF. Both were under 600 min^{-1}. The measured stator core temperature was used as the magnet temperature in the FEM analysis because the heat of the motor was low enough and the measurement time was short. While the measured no-load-induced back EMF was 151.1 Vrms, the calculated value was 155.4 Vrms. The error between the measured and calculated values was 2.9%, which was small enough, and confirmed the prototype was made as designed.

4.3. Measurement of peak power

The prototype in-wheel motor was installed in a test bench and a load test was conducted. The wheel side of the motor was fastened to the test bench, and direct current (DC) power and cooling oil were input and output from the inverter side. The DC voltage was 380 V. Figure 9 shows the measured waveforms of voltage and current at a peak output of 60 kW (600 min^{-1}, 960 Nm). Although the current waveform contains high-order pulsating components corresponding to the carrier frequency of the inverter, it was a substantial sine wave, and it was confirmed on the actual machine that the prototype in-wheel motor can be stably driven.

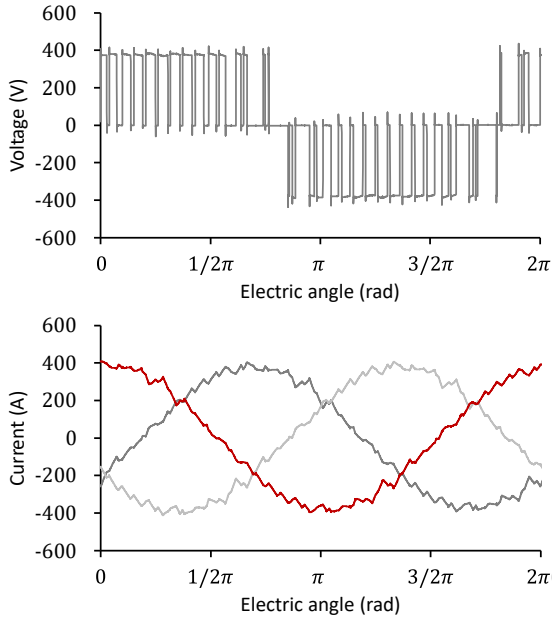

Fig. 9 Measured waveforms under peak output at 960 Nm and 600 min^{-1} (upper: voltage, lower: current).

5. CONCLUSION

We presented a strategy to increase power density of in-wheel system. We show that the output density can be improved by the synergistic effect of increasing the number of poles and the gap magnetic flux density.

To increase the gap magnetic flux density, we proposed a Halbach magnet array which combines main pole magnets, spoke magnets, and pole center cores. We also developed a rotor that includes our Halbach magnet array and determined the rotor's superiority to the conventional Halbach-array rotor with an SPM layout through FEM analysis and a magnetic circuit model. FEM analysis showed that our rotor can increase the gap magnetic flux density by 6.3% with 39% fewer magnets than the conventional rotor.

We fabricated a prototype in-wheel motor using the developed rotor and measured the no-load properties. The no-load-induced back EMF of the prototype motor was almost sinusoidal and was 151.1 Vrms, which is in good agreement with the calculated value of 155.4 Vrms. The peak output was 60 kW, verifying that stable driving is possible with the prototype in-wheel motor.

REFERENCES

(1) L. Shao, A. E. H. Karci, D. Tavernini, A. Sorniotti and M. Cheng, "Design approaches and control strategies for energy-efficient electric machines for electric vehicles — a review," *IEEE Access*, vol. 8, pp. 116900–116913, 2020.

(2) C. Chen, Y. Cheng and F. Meng, "Optimum design of a novel in-wheel suspension of the electric wheel," *in Proc. 3rd IEEE Int. Conf. on Green Energy and Applications*, p.106–110, 2019.

(3) A. Fatemi, D. M. Ionel, N. A. O. Demerdash and T. W. Nehl, "Optimal design of IPM motors with different cooling systems and winding configurations," *IEEE trans. Ind. Appl.*, vol. 52, no. 4, pp. 3041–3049, 2016.

(4) R. L. S. Nimmana and A. Chiba, "Design of high power density motor for EV applications," *in Proc. 21st Int. Conf. on Electrical Machines and Systems*, Oct. 2018.

(5) M. Degano, E. Carraro and N. Bianchi, "Selection criteria and robust optimization of a traction PM-assisted synchronous reluctance motor," *IEEE trans. Ind. Appl.*, vol. 51, no. 6, pp. 4383–4391, 2015.

(6) E. Carraro, M. Morandin and N. Bianchi, "Traction PMASR motor optimization according to a given driving cycle," *IEEE trans. Ind. Appl.*, vol. 52, no.1, pp. 209–216, 2016.

(7) A. Takahashi, S. Sugimoto, M. Ito, S. Tamiya, K. Fujii and M. Endo, "High-efficiency technology for railway-vehicle traction motors," *in Proc. 23rd Int. Conf. on Electrical Machines and Systems*, Nov. 2020.

(8) M. Ito, S. Sugimoto, A. Takahashi, S. Tamiya and T. Kushida, "A high strength rotor structure for IPMSM with narrow bridges," *in Proc. Int. Conf. on Electrical Machines*, Aug. 2020.

(9) Z. Ji, H. Li, Z. Chen, T. Yu, L. Liu and M. Ma, "Design and optimization of permanent magnet assisted synchronous reluctance motor for better torque performance," *in Proc. 22nd Int. Conf. on Electrical Machines and Systems*, Aug. 2019.

(10) C.-S. Jun and B.-I. Kwon, "Performance comparison of a spoke-type PM motor with different permanent magnet shapes and the same magnet volume," *J. IET Electr. Power Appl.*, vol. 11, no. 7, pp. 1196–1204, 2017.

(11) A. Fatemi, D. M. Ionel, M. Popescu, Y. C. Chong and N. A. O. Demerdash, "Design optimization of a high torque density spoke-type PM motor for a Formula E race drive cycle," *IEEE trans. Ind. Appl.*, vol. 54, no. 5, pp. 4343–4354, 2018.

(12) N. Morimura, H. Suzuki and M. Morishita, "Single Halbach field magnet designed from dual Halbach field magnet for rotating machines," *in Proc. 21st Int. Conf. on Electrical Machines and Systems*, Oct. 2018.

(13) L. Duan, H. Lu, C. Zhao and H. Shen, “Influence of different Halbach arrays on performance of permanent magnet synchronous motors,” *in Proc. IEEE Int. Conf. on Artificial Intelligence and Computer Applications*, June 2020.

(14) S. Alshibani, “Application of particle swarm optimization in the design of Halbach permanent magnet synchronous generators for megawatt level wind turbines,” *in Proc. 7th Int. Conf. on Renewable Energy Research and Applications*, Oct 2018.

(15) M. J. Bala, D. Roy and A. Sengupta, “The performance enhancement of BLDC motor using Halbach array rotor,” *in Proc. IEEE 1st Int. Conf. for Convergence in Engineering*, Sept. 2020.